polymer papers

Surface melting in melt-crystallized linear polyethylene

Y. Tanabe*, G. R. Strobl and E. W. Fischer
Institut für Physikalische Chemie der Universtät Mainz, and Max Planck Institut für Polymerforschung, Mainz D-65, Federal Republic of Germany
(Received 11 October 1985)

Morphological changes during the premelting of linear polyethylene were investigated by small-angle X-ray scattering using correlation-function analysis. The thickness of the amorphous regions, $\langle d_a \rangle$, showed a reversible change with temperature, which indicates presence of a local equilibrium state. During heating, the average thickness of lamellae $\langle d_c \rangle$ decreases first for temperatures below the initial crystallization temperature (T_c). The simultaneous decrease in $\langle d_c \rangle$ and increase in $\langle d_a \rangle$ provide evidence for a surface melting of the lamellae. Above T_c an irreversible thickness growth of the crystalline lamellae (increase of $\langle d_c \rangle$) is observed. It does not affect the thickness of the amorphous regions, which remains unchanged.

(Keywords: small-angle X-ray scattering; correlation function; linear polyethylene; premelting; lamellar thickness; amorphous state)

INTRODUCTION

The phenomenon that the crystallinity of semicrystalline polymers decreases continuously during heating up to the melting point is commonly referred to as 'premelting'. Various explanations for premelting have been offered. Fischer[1-4] and Zachmann[5,6] discussed a possible entropy change in the amorphous regions and considered an increase in thickness of amorphous regions as the cause[7]. A boundary melting mechanism leading to an increase in thickness of the amorphous regions was proposed. Alternatively, Flory[8], Killian[9-11], Asbach *et al.*[12] and Pope *et al.*[13] considered selective melting of small lamellae within the lamellar stacks as the origin of partial melting, thus explaining the observed change in long spacings. Possible effects of lattice distortions within crystallites, discussed in refs. 14–19, suggested that melting may start preferentially at lateral grain boundaries, assuming the existence of mosaic blocks in melting range. Finally, dealing with partial crystallization and melting of low-density polyethylene, Strobl *et al.*[20] proposed a new model in which crystallization occurs by a consecutive formation of lamellae in building up the lamellar stacks. Premelting is explained by a successive melting of the lamellae in reversed order.

In spite of the various explanations, morphological change during the melting process has not been really clarified. In particular, although most authors assume an equilibrium state for the amorphous phases, this has not yet been verified by experiments. The correlation-function analysis of small-angle X-ray scattering (SAXS) curves provides a means for checking this assumption. All main parameters of the lamellar structure such as long spacing, average thickness of crystalline and amorphous regions, crystallinity, the density difference between the two phases and the specific surface[3,4,21] can be simultaneously determined. This correlation function was introduced first by Debye[22] and developed further by Vonk *et al.*[23,24] for a one-dimensional system with transition regions. Strobl and Schneider[25] developed a technique for a direct evaluation of the structure parameters from the correlation function.

In this paper, the correlation function method was applied in a temperature-dependent experiment on samples of linear polyethylene (LPE), which were first crystallized at various temperatures. This enables a check of the equilibrium-state assumption for the amorphous phases. The complete premelting behaviour of LPE is discussed.

OUTLINE OF CORRELATION-FUNCTION ANALYSIS

Unoriented samples of a partially crystalline polymer can be represented by a structure model consisting of alternating parallel and flat crystalline and amorphous layers in randomly oriented clusters (lamellar two-phase structure). Dimensions of the clusters parallel and normal to the lamellar surfaces are assumed to be sufficiently large compared to the interlamellar distance. Uniformity of the sample is also assumed: all clusters should obey the same internal statistics.

The SAXS intensity of this system can be related to the one-dimensional correlation function $\gamma_1'(x)$, which describes the spatial correlations of the electron density fluctuations and is defined as the average

$$\gamma_1'(x) = \langle [\rho(x_0) - \langle \rho \rangle][\rho(x_0 + x) - \langle \rho \rangle] \rangle \qquad (1)$$

Here $\rho(x)$ denotes the electron-density distribution along a trajectory normal to the lamellae, $\langle \rho \rangle$ is the mean electron density and the angle brackets indicate averaging over all points x_0 within a cluster. The electron-density correlation function $\gamma_1'(x)$ can be normalized as

$$\gamma_1(x) = \gamma_1'(x)/\langle \rho^2 \rangle \qquad (2)$$

where $\langle \rho^2 \rangle = \langle (\rho(x_0) - \langle \rho \rangle)^2 \rangle$ is the average electron-

* Present address: Research Institute for Polymers and Textiles, 1-1-4 Higashi, Yatabe-machi, Tsukuba-gun, Ibaraki 305, Japan.

0032-3861/86/081147-07$03.00

density fluctuation. General scattering theory relates $\gamma_1'(x)$ or $\gamma_1(x)$ to the scattered intensity $I(s)$

$$\gamma_1'(x)=\int_0^\infty 4\pi s^2 I(s)\cos 2\pi sx\,ds \tag{3}$$

$$\gamma_1(x)=\frac{\int_0^\infty s^2 I(s)\cos 2\pi sx\,ds}{\int_0^\infty s^2 I(s)\,ds} \tag{4}$$

where $s=(2/\lambda)\sin\theta$, 2θ denoting the scattering angle and λ the X-ray wavelength.

Rather than changing sharply at the boundary between the crystalline and amorphous regions, the electron-density distribution $\rho(x)$ may show a smooth transition from the density ρ_c to ρ_a. Vonk[24] took account of the effect of such a transition layer. *Figure 1* shows $\rho(x)$ together with the corresponding correlation function $\gamma_1'(x)$ (ref. 25) in the case where the crystallinity ω_c is larger than 0.5. The value $\gamma_1'(0)$ is given by

$$\gamma_1'(0)=Q=\langle\rho^2\rangle=\left(\omega_c\omega_a-\frac{E}{3\langle L\rangle}\right)\Delta\rho^2 \tag{5}$$

where Q denotes the invariant, $\Delta\rho=\rho_c-\rho_a$, $\omega_a=1-\omega_c$, $\langle L\rangle$ is the number-average distance between the nearest-neighbour lamellae, and E is the thickness of transition layers. The depth A of the first minimum of $\gamma_1'(x)$ is given by

$$A=\omega_a^2\Delta\rho^2 \tag{6}$$

(for the case $\omega_c>0.5$; $A=\omega_c^2\Delta\rho^2$ for $\omega_c<0.5$). The slope $d\gamma_1'(x)/dx$ is

$$\frac{d\gamma'(x)}{dx}=-\frac{O_s}{2}\Delta\rho^2 \tag{7}$$

where O_s denotes the specific surface given by

$$O_s=2/\langle L\rangle \tag{8}$$

The invariant Q' for the associated ideal two-phase structure (with no transition layers) is given by extrapolating the slope to $x=0$.

$$Q'=\omega_c\omega_a\Delta\rho^2 \tag{9}$$

Extrapolation of this slope to the other side intersects the horizontal line of $\gamma_1'(x)=-A$ at $x=\langle d_a\rangle$, the number-average thickness of amorphous regions (if $\omega_c>0.5$; for $\omega_c<0.5$, $x=\langle d_c\rangle$, the number-average thickness of crystalline regions). The thicknesses of the two layers are related to $\langle L\rangle$ as follows:

$$\langle d_a\rangle=\omega_a\langle L\rangle \quad , \quad \langle d_c\rangle=\omega_c\langle L\rangle \tag{10}$$

The position of the first peak of the correlation function $\gamma_1(x)$ indicates the long spacing L, which means the most probable next-neighbour distances of lamellae. L differs from $\langle L\rangle$ when the distribution of the distances between nearest-neighbour lamellae is skewed.

In calculating the correlation functions experimentally, care must be taken over the following points. First, the liquid-like background should be subtracted[26]. In the scattering range of the experiment it turned out to be constant. Secondly, to eliminate termination effects on the Fourier transform, the SAXS curve has to be continued to infinity by using either[24]

$$I(s)\simeq\frac{d_1}{s^4}\left(\frac{\sin\pi sE}{\pi sE}\right)^2 \qquad (s\to\infty) \tag{11}$$

where $d_1=\lim_{s\to\infty} s^4 I(s)$ is a constant related to the specific surface O_s of the associated ideal two-phase model (Porod's law), or[27]

$$I(s)\simeq\frac{d_1}{s^4}\exp(-4\pi^2\sigma^2 s^2) \qquad (s\to\infty) \tag{12}$$

where σ is related to E by $E\simeq 3.4\sigma$. Equations (11) and (12) gave equivalent results. For the use of equation (11), constants d_1 and E must be given, which are determined by a plot of $\tilde{I}(s)s$ *versus* $1/s^2$ (ref. 24).

$$\tilde{I}(s)\simeq\frac{\pi d_1}{2}\left(\frac{1}{s^3}-\frac{2\pi^2E^2}{3s}\right) \qquad (s\to\infty) \tag{13}$$

Here $\tilde{I}(s)$ is the slit-smeared intensity after subtracting the liquid-like background scattering. As shown in *Figure 2*,

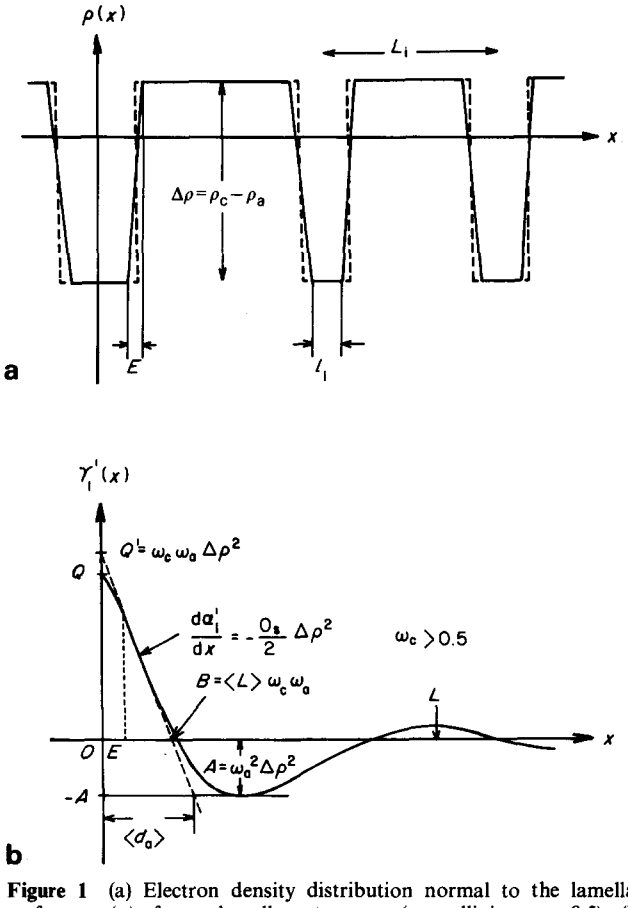

Figure 1 (a) Electron density distribution normal to the lamellar surfaces, $\rho(x)$, for a lamellar structure (crystallinity $\omega_c>0.5$). (b) Corresponding correlation function $\gamma_1'(x)$

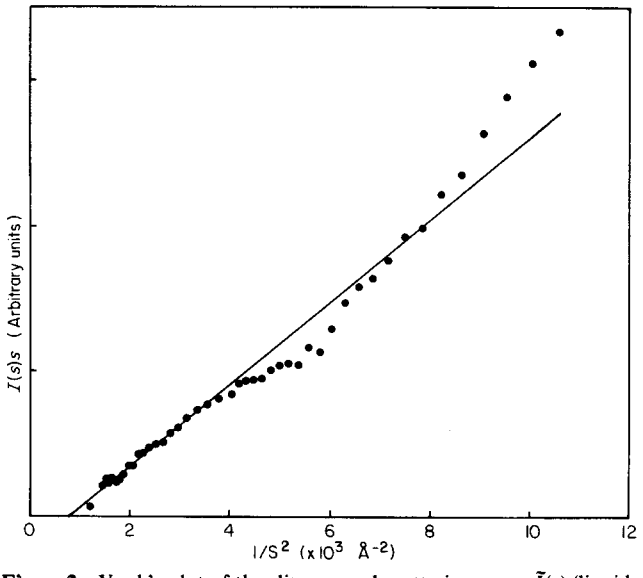

Figure 2 Vonk's plot of the slit-smeared scattering curve $\tilde{I}(s)$ (liquid-like background subtracted) for LPE crystallized and measured at 125°C

the linear portion corresponding to equation (13) exists at relatively high scattering angles (for example, $s \gtrsim 0.017$ Å^{-1}. The constants d_1 and E can be directly derived.

The effect of transition layers can be eliminated by multiplication of $I(s)$ with the factor $((\sin \pi sE)/\pi sE)^{-2}$. Then Fourier transformation gives the correlation function of the associated ideal two-phase model. Agreement of the results obtained before and after subtracting the effect of transition layers was satisfactory.

Thirdly, at small angles hole scattering and/or scattering from heterogeneities is superimposed on the observed intensity. We could not eliminate this effect experimentally. It affects the individual values Q, Q' and A but not the sum $Q'+A$. Therefore only $Q'+A$ is used here, which is related to ω_a and $\Delta\rho$ by

$$Q'+A=\omega_a\Delta\rho^2 \tag{14}$$

From the correlation function analysis, the values L, $\langle d_a \rangle$ and $Q'+A$ were determined as independent parameters. They are not sufficient for a complete characterization of the two-phase structure. Hence $\Delta\rho$ was taken from the literature. The electron density of crystalline regions ρ_c was given by Swan[28] as a function of temperature T(°C) and that of amorphous regions ρ_a by Richardson *et al.*[29]

$$\rho_c^{-1}\ (\mathrm{cm^3\,g}) = 0.9940 + 2.614\times10^{-4}T + 4.43\times10^{-7}T^2 \tag{15}$$

$$\rho_a^{-1}\ (\mathrm{cm^3\,g}) = 1.152 + 8.8\times10^{-4}T \tag{16}$$

EXPERIMENTAL

Samples of LPE (Lupolen 6011L) were prepared. They were crystallized at 125°C, 127°C and 131°C for four weeks after melting at 160°C for one day. After crystallization they were rapidly cooled to room temperature. The d.s.c. curves for these samples are given in *Figure 3*. The sample crystallized at 131°C has two peaks, reflecting a bimodal distribution of lamellae, which suggests that crystallization of small lamellae occurred during cooling.

The SAXS measurements were made with a Kratky camera by using Ni-filtered Cu Kα radiation, a xenon-filled proportional counter and a pulse-height discriminator. Absolute values of the scattered intensity were determined by a standard sample[30]. The corrections for the slit-like collimation were made by Strobl's method[31]. The sample temperature was raised in steps and controlled within ±0.2°C. The SAXS measurements were started after holding for 3 h at each temperature.

RESULTS AND DISCUSSION

The desmeared scattering curves $I(s)s^2$ determined for a series of temperatures during heating the sample crystallized at 125°C are shown in *Figure 4*. The intensity of the first peak increases with temperature. The derived correlation functions $\gamma_1(x)$ are shown in *Figure 5a*. *Figure 5b* shows the correlation functions derived from the SAXS curves measured during the successive cooling. The parameters L, $\langle d_a \rangle$, $Q+A$ and $Q'+A$ directly obtained

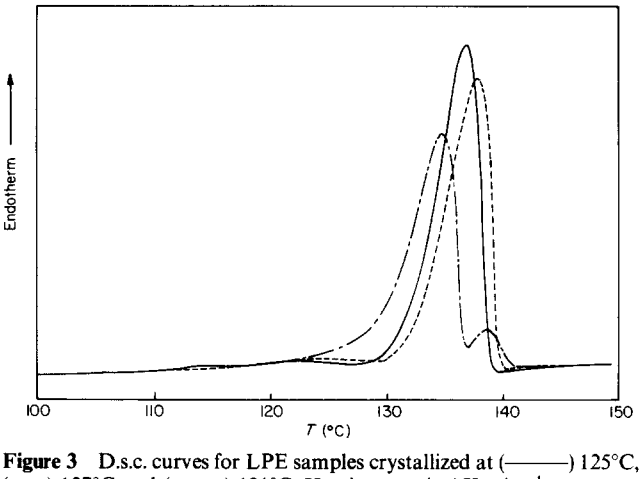

Figure 3 D.s.c. curves for LPE samples crystallized at (———) 125°C, (– – –) 127°C and (–·–·–) 131°C. Heating rate is 4 K min^{-1}

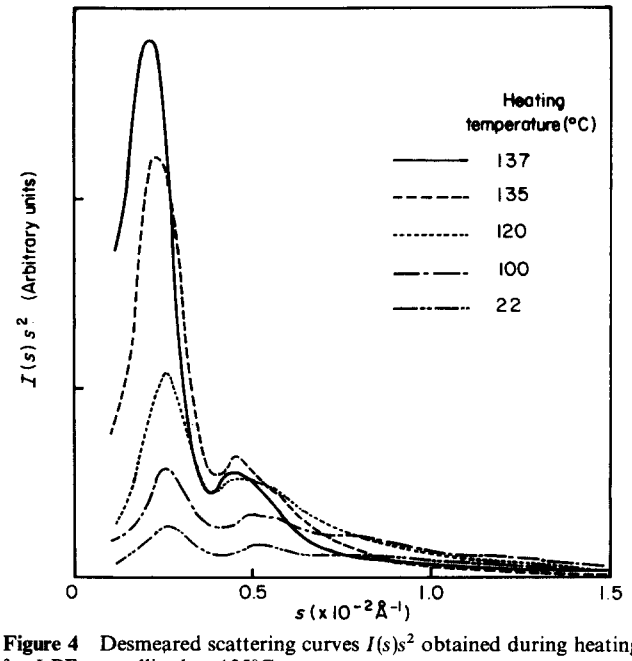

Figure 4 Desmeared scattering curves $I(s)s^2$ obtained during heating for LPE crystallized at 125°C

from the correlation functions for all samples under study are summarized in *Table 1*.

The temperature dependence of $\langle d_a \rangle$ is shown in *Figure 6*. It is important to note that $\langle d_a \rangle$ changes almost reversibly, slight differences being observed only in the neighbourhood of the initial crystallization temperature T_c. Below 100°C the change in $\langle d_a \rangle$ is strictly reversible, and does not depend on the thermal history of specimen like the choice of T_c and the cooling rate after crystallization. *Figure 7* represents the temperature

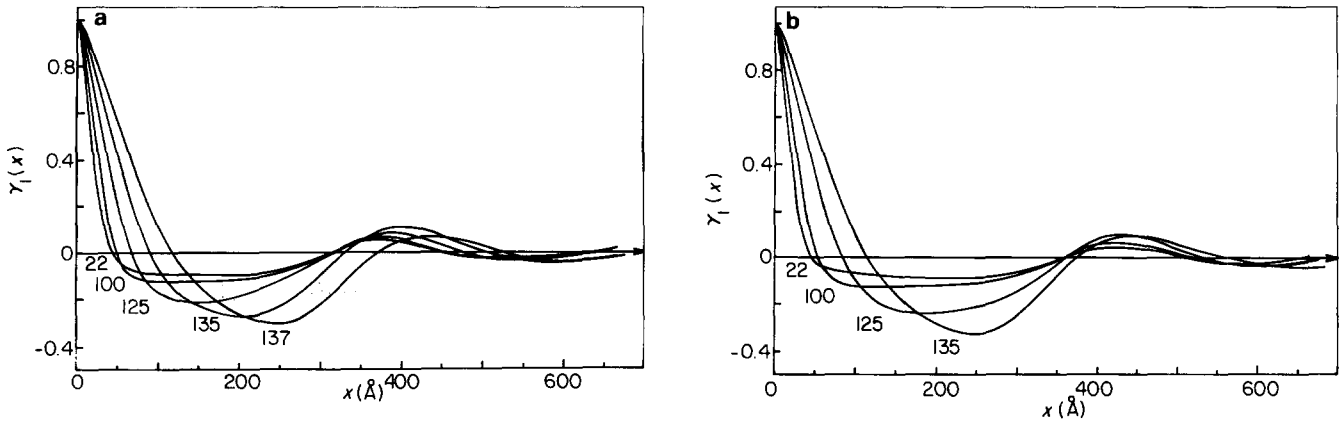

Figure 5 Correlation functions $\gamma_1(x)$ obtained during heating (a) and cooling (b) for LPE crystallized at 125°C (temperatures are marked on the curves in degrees Celsius)

Table 1 Temperature dependence of structure parameters of LPE derived from the electron-density correlation function

	Temperature (°C)	L (Å)	$\langle d_a \rangle$ (Å)	$10^3 (Q+A)$ $\left(\frac{\text{mol electron}}{\text{cm}^3}\right)^2$	$10^3 (Q'+A)$ $\left(\frac{\text{mol electron}}{\text{cm}^3}\right)^2$
PE crystallized at 125°C					
Heating	22	366	32.8	0.695	0.740
	81	376	40.9	0.991	1.074
	100	374	46.3	1.175	1.254
	120	382	64.0	1.693	1.796
	125	388	71.5	1.855	1.960
	135	400	101.1	2.590	2.715
	137	438	134.0	3.055	3.176
Cooling	135	442	134.7	2.940	3.040
	125	430	90.6	2.070	2.167
	120	424	76.4	1.739	1.817
	100	426	50.3	1.117	1.185
	81	432	42.6	0.903	0.962
	22	422	35.1	0.648	0.674
PE crystallized at 127°C					
Heating	22	368	31.9	0.677	0.697
	81	380	39.4	0.923	0.986
	100	390	46.0	1.103	1.178
	120	388	66.0	1.643	1.729
	127	398	81.1	1.982	2.079
	135	414	114.1	2.638	2.747
	137	484	167.2	3.168	3.273
Cooling	135	490	169.0	3.224	3.332
	127	462	105.4	2.288	2.383
	100	448	49.2	1.093	1.171
	22	449	32.8	0.638	0.665
PE crystallized at 131°C					
Heating	22	284	36.8	0.851	0.905
	81	290	43.9	1.175	1.268
	100	288	48.6	1.377	1.477
	120	290	63.2	1.827	1.940
	131	314	88.0	2.465	2.607
	135	374	125.9	2.898	3.017
	137	496	181.2	3.033	3.127
Cooling	135	520	187.1	3.132	3.210
	131	488	143.3	2.753	2.840
	120	476	78.6	1.704	1.784
	100	478	50.1	1.076	1.138
	81	470	43.0	0.860	0.914
	22	470	34.5	0.589	0.618

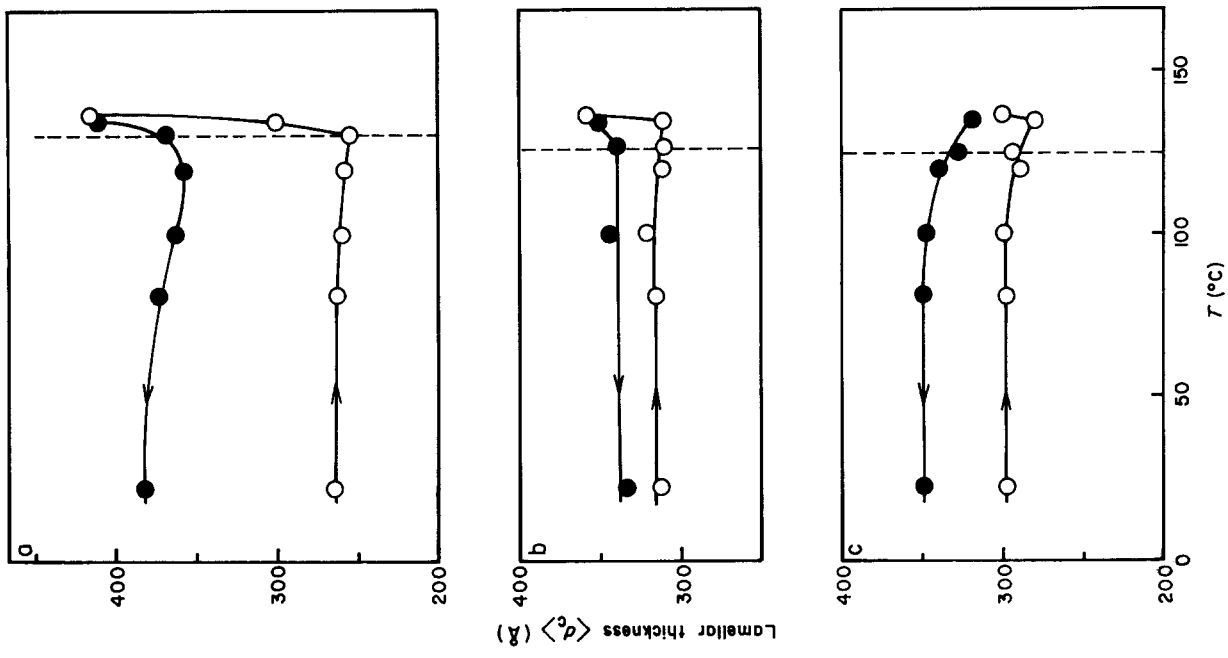

Figure 8 Temperature dependence of the mean crystalline thickness $\langle d_c \rangle$. Samples crystallized at (a) 131°C, (b) 127°C, (c) 125°C

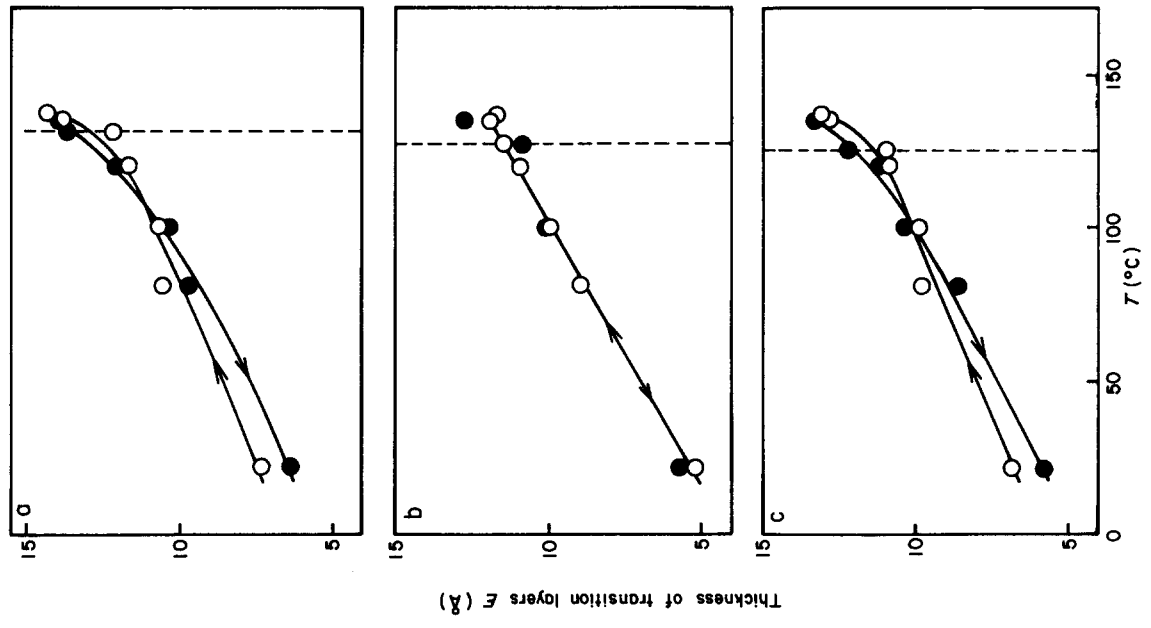

Figure 7 Temperature dependence of the thickness of transition layers E. Samples crystallized at (a) 131°C, (b) 127°C, (c) 125°C

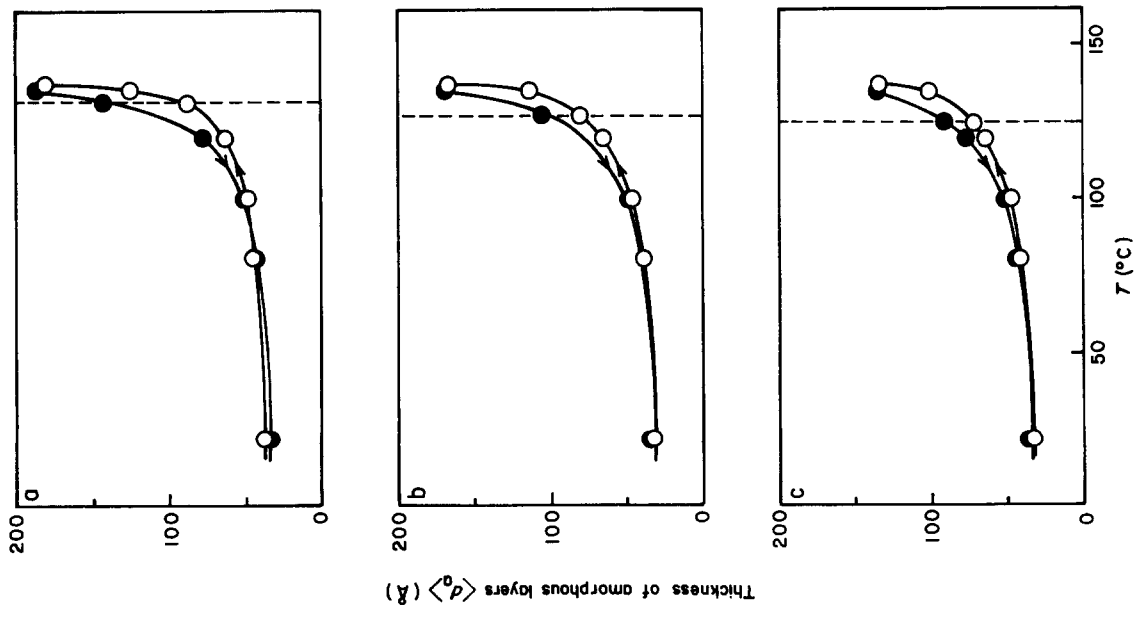

Figure 6 Temperature dependence of the average thickness of amorphous layers $\langle d_a \rangle$ during heating (○) and cooling (●). LPE samples crystallized at (a) 131°C, (b) 127°C, (c) 125°C

dependence of E, which is also reversible. All these results suggest that the amorphous regions in melt-crystallized LPE are in a state of local equilibrium. This has been assumed by various authors and is proved here by the SAXS experiment.

Figure 8 shows the temperature dependence of $\langle d_c \rangle$. There is first a decrease and then an irreversible increase starting several degrees above T_c. The decrease of $\langle d_c \rangle$ reflects a surface melting and appears to be smaller than the increase of $\langle d_a \rangle$, thus resulting in an increase of $\langle L \rangle$ (*Figure 10*). This observation is not accounted for by the existing models. The detailed molecular mechanism will have to be discussed further on.

Above T_c, a drastic increase in L (*Figure 9*), $\langle L \rangle$ (*Figure 10*) and $\langle d_c \rangle$ (*Figure 8*) is observed. It indicates a lamellar thickness growth by melting and/or recrystallization or solid diffusion of the chains. As expected and confirmed by the data, this growth is irreversible. It is important to note that this irreversible change in the crystalline thickness does not affect the thickness of the amorphous layers. In contrast to $\langle d_c \rangle$, $\langle d_a \rangle$ shows a fully reversible behaviour,

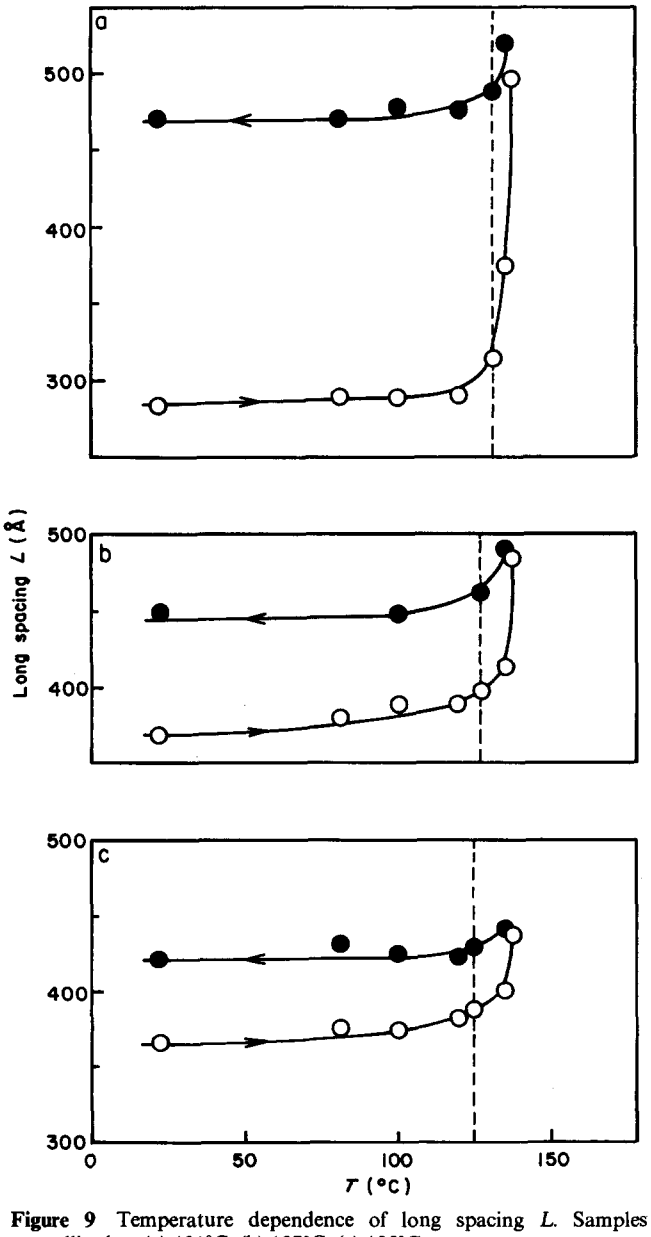

Figure 9 Temperature dependence of long spacing L. Samples crystallized at (a) 131°C, (b) 127°C, (c) 125°C

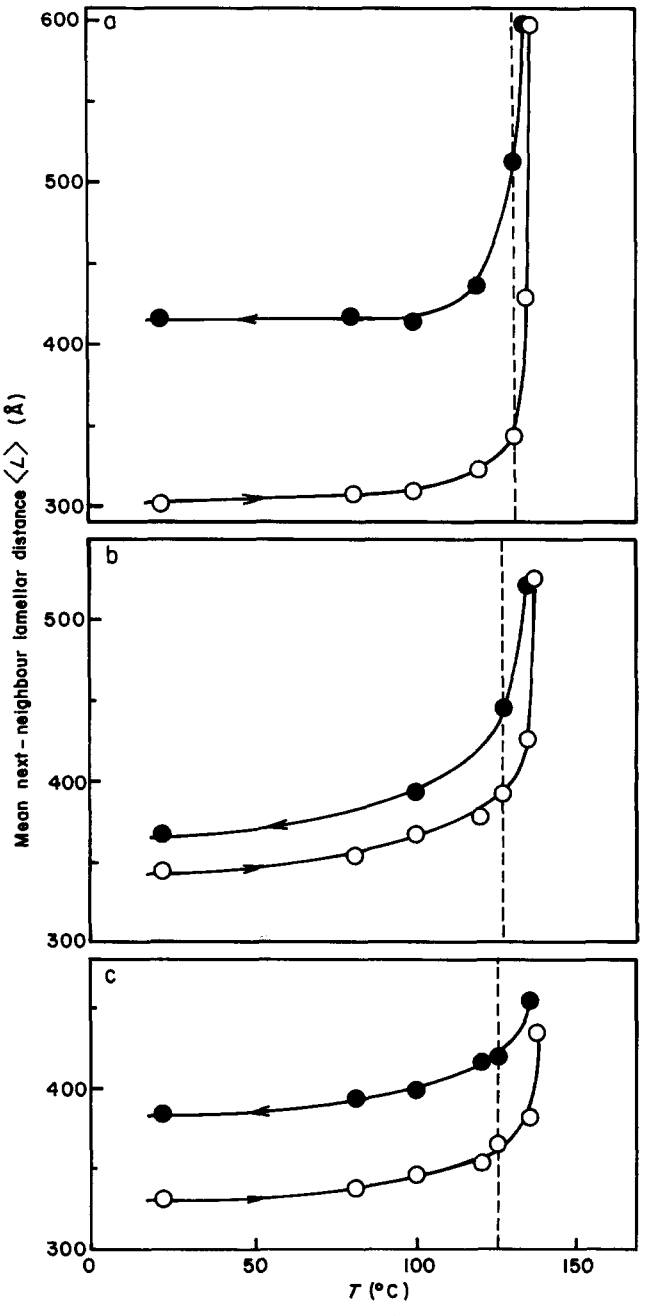

Figure 10 Temperature dependence of the mean next-neighbour lamellar distance $\langle L \rangle$. Samples crystallized at (a) 131°C, (b) 127°C, (c) 125°C

lending support to the notion of local equilibrium established in the amorphous layers.

Compared with the change in L (the most probable next-neighbour distance of lamellae), the change observed for $\langle L \rangle$ (the number-average distance) is larger (*Figures 9, 10*). This means that the distribution of next-neighbour distances of lamellae becomes asymmetrical upon crystal formation during cooling.

The crystallinity ω_c decreases continuously with temperature (*Figure 11*). This continuous change has to be associated with both surface melting and successive melting of whole crystallites.

ACKNOWLEDGEMENTS

Thanks are due to Professor Dr G. Kanig (BASF AG, Ludwigshafen am Rhein) for supplying crystallized

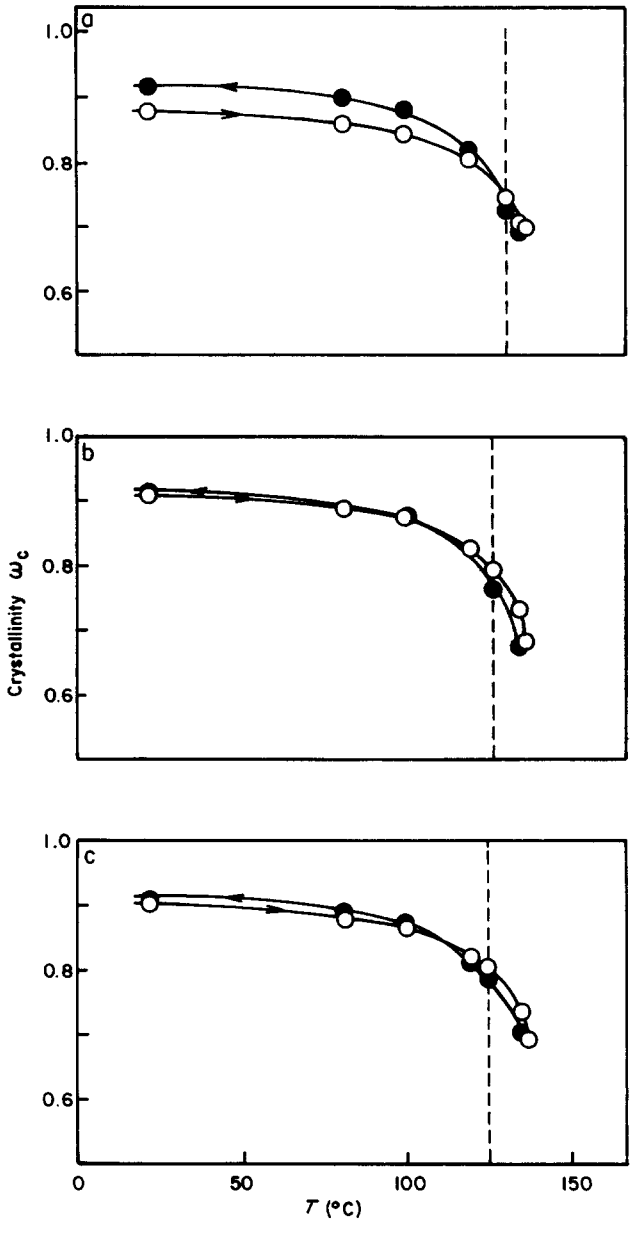

Figure 11 Temperature dependence of the crystallinity ω_c. Samples crystallized at (a) 131°C, (b) 127°C, (c) 125°C

samples of LPE. The work was supported by the Deutsche Forschungsgemeinschaft (Sonderforschungsbereich 41 Mainz/Darmstadt).

REFERENCES

1 Fischer, E. W. *Kolloid-Z.Z. Polym.* 1967, **218**, 97
2 Fischer, E. W. *Kolloid-Z.Z. Polym.* 1969, **231**, 458
3 Fischer, E. W. *Pure Appl. Chem.* 1971, **26**, 385
4 Fischer, E. W. in 'Proc. IUPAC Macromolecular Microsymposia V III, Prague', 1971, p. 113
5 Zachmann, H. G. *Kolloid-Z.Z. Polym.* 1967, **216/217**, 180
6 Zachmann, H. G. *Kolloid-Z.Z. Polym.* 1969, **231**, 504
7 Fischer, E. W., Martin, R., Schmidt, G. F. and Strobl, G. R. in *Prepr. IUPAC Symposium, Toronto* 1968, A6–17
8 Flory, P. J. *J. Chem. Phys.* 1949, **17**, 223
9 Kilian, H. G. *Kolloid-Z.Z. Polym.* 1967, **215**, 131
10 Kilian, H. G. *Kolloid-Z.Z. Polym.* 1967, **216/217**, 192
11 Kilian, H. G. *Kolloid-Z.Z. Polym.* 1969, **231**, 534
12 Asbach, G. I., Kilian, H. G. and Müller, F. H. *J. Polym. Sci.* 1967, **C18**, 133
13 Pope, D. P. and Keller, A. *J. Polym. Sci., Phys. Sci. Edn.* 1967, **14**, 821
14 Sanchez, I. C. and Eby, R. K. *J. Res. Natl. Bur. Stand.* 1973, **77A**, 353
15 Petermann, J., Miles, M. and Gleiter, H. *J. Macromol. Sci.* 1976, **B12**, 393
16 Yeh, G. S. Y., Hosemann, R., Loboda-Čačković, J. and Čačković, H. *Polymer* 1976, **17**, 309
17 Hosemann, R., Lindenmeyer, P. H. and Yeh, G. S. Y. *J. Macromol. Sci.* 1978, **B15**, 19
18 Haase, J., Hosemann, R. and Köhler, S. *Polymer* 1978, **19**, 1358
19 Haase, J., Köhler, S. and Hosemann, R. *Z. Naturforsch.* 1978, **33a**, 1472
20 Strobl, G. R., Schneider, M. J. and Voigt-Martin, I. G. *J. Polym. Sci., Polym. Phys. Edn.* 1980, **18**, 1361
21 Fulcher, K. U., Brown, D. S. and Wetton, R. E. *J. Polym. Sci.* 1972, **C38**, 315
22 Debye, P., Anderson, H. R. Jr. and Brumberger, H. *J. Appl. Phys.* 1957, **28**, 679
23 Vonk, C. G. and Kortleve, G. *Kolloid-Z.Z. Polym.* 1967, **220**, 19
24 Vonk, C. G. *J. Appl. Crystallogr.* 1973, **6**, 81
25 Strobl, G. R. and Schneider, M. J. *J. Polym. Sci., Polym. Phys. Edn.* 1980, **18**, 1343
26 Tanabe, Y., Müller, N. and Fischer, E. W. *Polym. J.* 1984, **16**, 445
27 Ruland, W. *J. Appl. Crystallogr.* 1971, **4**, 70
28 Swan, P. R. *J. Polym. Sci.* 1960, **42**, 525
29 Richardson, M. J., Flory, P. J. and Jackson, J. B. *Polymer* 1963, **4**, 221
30 Kratky, O., Pilz, I. and Schmetz, P. J. *J. Colloid Interface Sci.* 1966, **21**, 24
31 Strobl, G. R. *Acta Crystallogr.* 1970, **A26**, 367